J Mater Sci: Mater Med (2008) 19:2679–2689
DOI 10.1007/s10856-008-3398-1

Mulberry non-engineered silk gland protein vis-à-vis silk cocoon protein engineered by silkworms as biomaterial matrices

Joydip Kundu · Moumita Dewan · Sarani Ghoshal · S. C. Kundu

Received: 31 October 2007 / Accepted: 31 January 2008 / Published online: 19 February 2008

Abstract Silk fibroin from silk gland of *Bombyx mori* 5th instar larvae was utilized to fabricate films, which may find possible applications as two-dimensional matrices for tissue engineering. *Bombyx mori* cocoon fibroin is well characterized as potential biomaterial by virtue of its good mechanical strength, water stability, thermal properties, surface roughness and biocompatibility. The present study aims to characterize the biophysical, thermal, mechanical, rheological, swelling properties along with spectroscopic analysis, surface morphology and biocompatibility of the silk gland fibroin films compared with cocoon fibroin. Fibroin solutions showed increased turbidity and shear thinning at higher concentration. The films after methanol treatment swelled moderately and were less hydrophilic compared to the untreated. The spectroscopic analysis of the films illustrated the presence of various amide peaks and conformational transition from random coil to β sheet on methanol treatment. X-ray diffraction studies also confirmed the secondary structure. Thermogravimetric analysis showed distinct weight loss of the films. The films were mechanically stronger and AFM studies showed surfaces were rougher on methanol treatment. The matrices were biocompatible and supported L929 mouse fibroblast cell growth and proliferation. The results substantiate the silk gland fibroin films as potential biomaterial matrices.

Abbreviations

SF	Silk fibroin protein
BMG	*Bombyx mori* gland
BMC	*Bombyx mori* cocoon
FTIR	Fourier transform infrared
XRD	X-ray diffraction
AFM	Atomic force microscopy

J. Kundu · M. Dewan · S. Ghoshal · S. C. Kundu (✉)
Department of Biotechnology, Indian Institute of Technology, Kharagpur 721302, India
e-mail: kundu@hijli.iitkgp.ernet.in

1 Introduction

Silk gland proteins present in the last larval stage of the silkworms produce threads of silky material to form the cocoon. Silk glands are mainly composed of three parts: the anterior, the middle, and the posterior silk glands, each playing different roles in silk secretion. Silk sericin protein, which coats the silk core fibroin protein, is secreted exclusively by the middle silk gland, the thickest part of the silk gland [1–3]. The longest suborgan, the posterior silk gland, is responsible for the synthesis of the silk core fibroin protein, which moves to the middle silk gland where molecules of sericin are added, then toward the anterior silk gland where the silk fiber is formed and spun into cocoons [4]. Silk fibroin protein is a representative fibril-forming protein that is synthesized in cells located on the surface of the posterior part of the silk gland in the silkworm *Bombyx mori*. It is subsequently secreted into the lumen and transported to the middle part of the silk gland for storage until required for spinning [5].

The silk fibroin protein (SF) matrices, with high specific surface area, high porosity and good biocompatibility [6], and biodegradability [7] have extensive applications in the field of biomaterials such as tissue scaffolds and drug delivery [8–10]. Silks can be processed into various forms including gels [11], powders [12], fibers [13], and membranes [14], scaffolds [15], hydrogels [16] and nanoparticles [17]. Although silks have been used thousand of years, interest in membranes has grown only within the last few decades. Transparent membranes of silk fibroin protein

have been processed with liquid silk from the gland [18], as well as solutions made with silk fibers dissolved in alkali salt solutions [19, 20] other types of solutions [21, 22] and organic solvents [23, 24]. A variety of processes have been employed in fabrication of the membranes. These include casting followed by air-drying [25] or freeze-drying [26], Langmuir–Blodgett technique [27] and layer-by-layer deposition [28].

There are several reports on the silk fibroin proteins of *B. mori*, *Antheraea yamamai* [29], *Antheraea pernyi* [30], *Antheraea mylitta* [31], *Dictyoploca japonica* [32], compared to work on *B. mori* sericin protein [33]. Silk membranes have been investigated for controlled release of drugs [10, 34and 35] and as platform for culturing animal cells [14, 15]. Membranes also have been used as materials for the study of the Silk I, Silk II and amorphous conformations as well as the transformations among them under the influence of the processing and post processing parameters. Spectroscopic, density, contact angle, crystallinity and microscopic measurements have been made. Other properties, such as mechanical, swelling, thermal as well as the diffusion and solubility of small molecules, have been measured because of their relevance to potential applications.

In this report the possibility of exploitation of mulberry non-engineered silk gland fibroin protein as biomaterial matrices was examined by determining their biophysical characteristics, surface morphology, thermal, mechanical, rheological, swelling properties and biocompatibility using fibroblast cell culture.

2 Materials and methods

2.1 Materials

Mulberry silkworm *B. mori* matured 5th instar larvae just before spinning and fresh live cocoons were collected from Debra Sericulture farm, West Midnapore, West Bengal, India. The DMEM (GIBCO, USA), fetal bovine serum (Hyclone), lithium bromide, L-glutamine, sodium bicarbonate and penicillin/streptomycin (Himedia laboratories Mumbai) were purchased. All other chemicals used in the experiments are of analytical grades.

2.2 Preparation of silk protein fibroin aqueous solution

The silk fibroin protein solutions were prepared from the cocoons of *B. mori* with slight modification of the procedure [36]. Cocoons of the *B. mori* were cut into small pieces and boiled with 0.02 M Na_2CO_3 for 60 min and washed with Milli Q water several times to remove the glue-like sericin proteins from the silk fibers. The degummed silk fibers were then dried in laminar hood for 24 h. They were dissolved in 9.3 M LiBr at 60°C for 4 h. The regenerated silk fibroin solution was dialyzed in a cellulose tube (12 KDa, MWCO) against deionized water for 48 h with several changes to remove the lithium bromide. The final concentration of the fibroin solution was kept about 6% (w/v), which was determined gravimetrically after drying fibroin solution at 60°C (Fig. 1a).

2.3 Preparation of silk gland fibroin protein solution and film fabrication

The silk gland fibroin protein solution was isolated from the mature silk gland of 5th instar larvae of *B. mori*. The intact silk

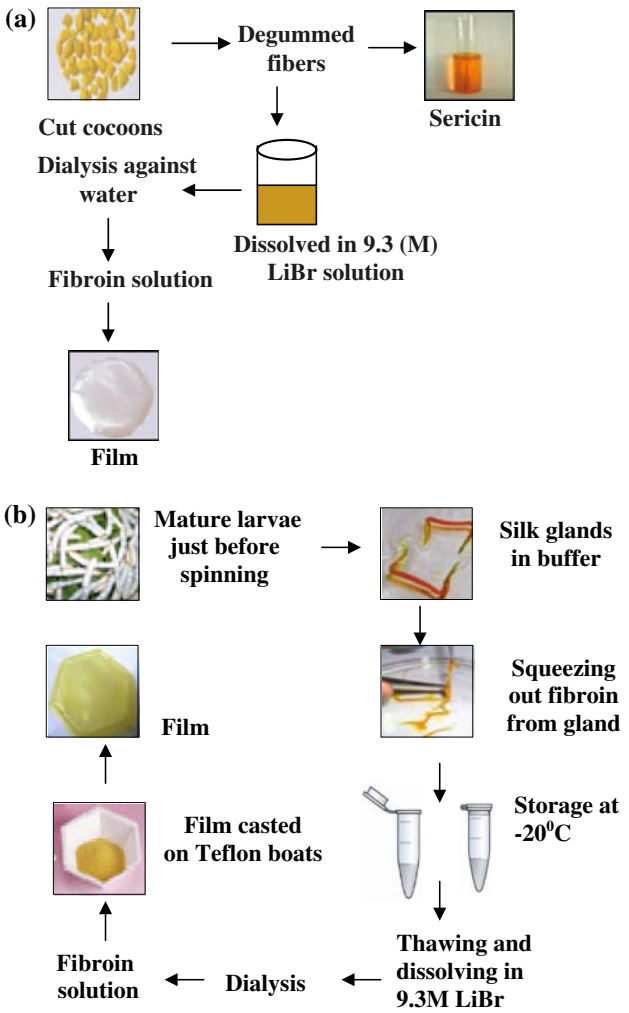

Fig. 1 (**a**) Schematic diagram for isolation of silk proteins from cocoons of *Bombyx mori* and film fabrication. (**b**) Schematic representation of the preparation of silk fibroin solution from *Bombyx mori* 5th instar silk gland and film fabrication

gland of mature 5th instar larvae was placed in phosphate buffer (pH 7.4) for removal of the glue like silk protein sericin that binds the fibroin. The protein was squeezed to separate the fibroin from the gland membrane. The silk fibroin protein isolated from the gland was either used immediately or was stored at −20°C in eppendorf tubes till further use.

The frozen silk gland fibroin protein was then thawed at room temperature and dissolved in 9.3 M LiBr at 37°C for 1 h. The regenerated silk fibroin solution was dialyzed in a cellulose tube (12 kDa MWCO) against deionized water for 24 h with several changes to remove the lithium bromide. The final concentration of the fibroin solution was about 1–2% (w/v), which was determined gravimetrically after drying fibroin solution at 37°C.

The fibroin films were prepared by casting on teflon-coated moulds. The regenerated silk gland fibroin protein solutions were casted on the teflon-coated boats at room temperature. After 24 h, the dried films were removed from the mould and stored at room temperature at 60% relative humidity until further studies. The films were accurately observed and checked for possible imperfection upon their removal from the moulds (Fig. 1b).

2.4 Turbidity measurements

Turbidity was calculated after measuring the transmittance at 500 nm with UV VIS spectrophotometer (Lambda 25, Perkin Elmer Instruments, USA) as a function of silk fibroin concentration given by the Equation:

$$\tau = -(\ln T)/c$$

where τ is the turbidity, T is the transmittance at 500 nm and c is the cell length.

2.5 Film swelling and water uptake of the films

The film swelling properties were evaluated by determining the swelling index. Each film samples were cut into dimensions of 10 × 10 mm and the studies were conducted in simulated phosphate buffer saline (pH 7.4) Each film sample was weighed and placed on a pre-weighed stainless steel wire mesh (600 micron sieve size). It was then submerged into phosphate buffer saline, pH 7.4 placed in a suitable container. After immersion the films were wiped off from the excess surface water using the filter paper and weighed. The increase in weight of the film was determined at preset time intervals (4 h is kept constant in this experiment) and determined after a constant weight was observed. Each measurement was repeated four times. The degree of swelling was calculated using the following Equation:

$$\text{Swelling index} = (Wt - Wo)/Wo,$$

where, Wt is the weight of film at time t, and Wo is the weight of film at time zero.

2.6 Fourier transform infrared spectroscopy (FTIR) analysis

The FTIR spectra of the silk fibroin thin films were obtained using Nicolet FT-IR spectrophotometer (Nexus-870). To avoid the effect of moisture the samples were dried overnight in a dessicator. The IR spectra in the absorbance mode were obtained in the spectral regions of 1000–4000 cm^{-1}. Each spectrum of the samples was acquired by accumulation of 32 scans with a resolution of 4 cm.

2.7 X-ray diffraction (XRD)

Wide-angle XRD patterns of the silk protein fibroin films were measured by a X-Ray diffractometer (PANalytical, X'Pert PRO PW3040/60) using Cu Kα radiation ($\lambda = 1.54$ Å) in the 2θ range of 10–60° at 40 kV, 30 mA. The measurements were performed at room temperature with samples spread on a conventional glass sample holder.

2.8 Raman spectroscopy

Raman spectra were acquired using a Renishaw System RM 1000B Laser Raman Micro Spectrometer coupled with a Leica DMLM microscope and thermoelectrically Peltier cooled charged coupled device detector. Excitation of sample was achieved with a 20 mW Ar Ion Laser source of 514 nm wavelength and filtering of the Rayleigh scattering was achieved through an edge filter at 200 cm^{-1} cut off that allows study of Raman scattering only on the Stokes side of the spectrum. Power at incidence on the sample surface was about 6 mW (100% laser power) with laser spot size of about 1.5 μm with 50× objectives.

Dispersion of the Raman scattered beam was achieved through a prism and an 1800 l/mm grating with motorized movement. The system was calibrated with Ne lamp and accuracy of peak position was constantly checked with Si standard. Spectra were acquired with the Windows Raman Environment (WiRE) software designed by the manufacturer. Display of the spectral trace (Raman Shift in cm^{-1} versus intensity in arbitrary units) and arithmetical calculations (peak fitting, parameter estimation, base line corrections and other analyses) were done with the GRAMS (Galactic) software. Acquisition of spectra was

made in the extended scanning mode in the range of 1800–800 cm^{-1} shifts from the Laser line.

2.9 Atomic force microscopy (AFM)

An optical lever type of AFM was used in the non-contact mode at ambient conditions. Small pieces of the membranes were mounted on the sample holder with two-sided tape. Images were obtained with a constant force of approximately 10^{-10}–10^{-9} N. Cantilevers with a silicon nitride tip of approximately 50 nm radius were used. The scanning rate was 0.600 lps. Measurements of the observed features were made using image processing and Data analysis software version 2.1.15 built into the AFM operating system. Since the dimensions covered a broad range, the approximate minima and maxima are presented.

2.10 Rheological properties of silk fibroin solutions

Shear viscosity of silk fibroin solutions was monitored using rheometric expansion system Brookfield Rotational Viscometer DV-II+ system, as a function of speed range from 0.0 to 100 RPM with LV-4 spindle having a spindle multiplier constant value of 640.

2.11 Dynamic contact angle

The contact angle of *B. mori* gland (BMG) film was estimated by the method of Dynamic Contact Angle, with a computer controlled automatic tensiometer (DCAT 11, Data physics). Both the advancing and the receding angles were determined from the experiment. Film strips of size 10 mm by 40 mm were first treated with ethanol. This induces the conformational change from random coil to beta sheets in fibroin. Each film was immersed in ethanol and air-dried. This was repeated for around 5 min. Both *B. mori* treated and untreated silk gland fibroin films were tested for their contact angle.

2.12 Mechanical properties

Mechanical properties of the films were evaluated at room temperature using the Hounsfield Tensiometer (H25 KS) equipment with a 100 N load cell [37]. Film strips in dimensions of 25 × 10 mm with uniform thickness, were held between two clamps positioned at a distance of 15 mm. Thick paper was attached on the surface of the clamp to prevent the film from being cut by the grooves of the clamp. Pulling the top clamp at a rate of 1 mm/min the measurements carried out. The tensile strength, elastic modulus and percentage elongation at break was recorded. Measurements for each film were carried out on four replicates.

2.13 Thermogravimetric analysis (TGA)

The silk gland fibroin films (both treated and untreated) were cut into small pieces weighing around 4–5 mg. Thermal gravimetric analysis (Pyris Diamond TG-DTA) was used to measure changes in weight of the films with increasing temperature. TGA curves were obtained under nitrogen atmosphere with a gas flow of 100 mL/min. The experiments were performed in an alumina crucible at a heating rate 20°C/min and run from 35 to 700°C.

2.14 Cell culture and MTT assay

L929 mouse fibroblast cells were maintained in DMEM medium supplemented with 10% fetal bovine serum, 200 mM L-glutamine, 2 mg ml^{-1} sodium bicarbonate, and 100 μg ml^{-1} penicillin/streptomycin. The cells were cultured in 25 cm^2 flasks at 37°C in a humidified atmosphere of 5% CO_2. Confluent monolayers were split by treatment with sterile phosphate-buffered saline (PBS) and 0.05% trypsin/EDTA solution, and the culture medium was replaced every 3 days. Silk gland protein fibroin solutions were filtered with 0.22 μm syringe filter and caste on 24-well tissue culture plate wells to obtain very thin films on the bottom portion of the wells. The circular matrices/films were sterilized with 70% alcohol under ultraviolet light overnight and then rinsed extensively three times with sterile PBS. The wells were then incubated with 0.2% BSA to block the uncoated well surface and then washed three times with sterile PBS. Before cell culturing, the protein-coated wells were pre-wetted by immersion in DMEM for 12 h in the 37°C incubator. Cells were trypsinized, counted, and plated at a density of 10^4 cells per ml of DMEM into the pre-wetted protein coated 24-well culture plates in triplicates and single factor analysis of variance (ANOVA) technique was used to assess statistical significance of results. After culturing for 1, 3, 5 days, the samples were examined with an inverted microscope (Leica) after day 1, 3, 5 respectively.

MTT assay is a quantitative colorimetric assay for mammalian cell survival and cell proliferation. It is an indirect method for assessing cell growth and proliferation, since mitochondria oxidize the MTT solution, giving a typical blue–violet end-product, O.D. value of 595 nm can be quantified to cell number. L929 mouse fibroblast cells were cultured inside the samples ($n = 3$) of silk gland

protein fibroin solutions for 5 days, and then the culture medium was replaced with serum free culture medium containing MTT (0.5 mg ml^{-1}). The 24-well tissue culture plates were then incubated at 37°C in the incubator for 4 h. The tissue culture plates were centrifuged for 5 min at 1700 rpm, and then the supernatant was aspirated. After that DMSO was added into each well of the tissue culture plate. The solution of each sample was aspirated into a microtiter plate (96-well tissue culture plates) and the absorbance at 595 nm was measured on a microplate reader (Bio Rad, model 550)

3 Results and discussion

3.1 Turbidity measurements

Turbidity is a consequence of intense light scattering associated with colloidal suspension of colloids in solvents. Turbidity is proportional to the both molecular weight and concentration of the particles in the system. Higher protein concentration leads to more and larger aggregates thus reflect more light hence higher turbidity and the solutions are opaque [38]. In order to examine the stability of silk fibroin solutions obtained from two different sources, the turbidity was calculated from the transmittance at 500 nm and was plotted with increasing silk fibroin protein concentrations from 0.1 to 1% w/v. Figure 2 shows the turbidity of silk fibroin aqueous solutions obtained from *B. mori* gland and cocoon respectively (each point on the curve represents an average of three measurements ± SD). With an increase of the silk fibroin concentration, turbidity of silk fibroin aqueous solutions obtained from *B. mori* gland increased markedly and became opaque at higher concentration. On the other hand, turbidity of the silk fibroin aqueous solutions obtained from *B. mori* cocoon was significantly less with an increase of concentration and remained transparent, indicating the solution is stable throughout a certain concentration. When silk fibroin is dissolved in 9.3 M LiBr solution, silk fibroin solution becomes viscose and transparent. During the dialysis LiBr are removed from the dialysis tube and regenerated aqueous silk fibroin solutions is prepared. Since silk fibroin is composed of mostly hydrophobic amino acids, fibroin molecules in aqueous solution aggregate and entangle each other by hydrophobic interactions [39, 40].

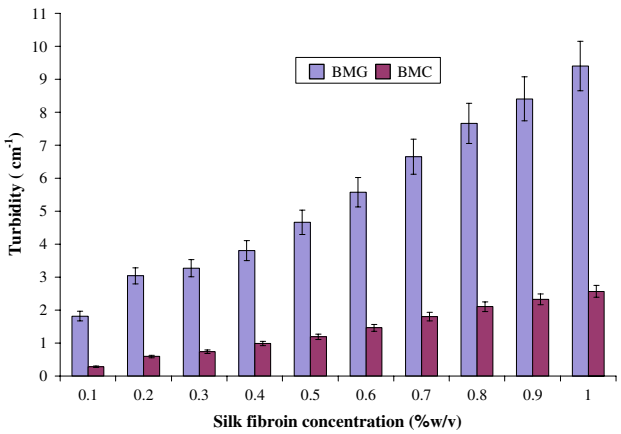

Fig. 2 Turbidity of the regenerated silk fibroin protein solutions from *Bombyx mori* gland and cocoon

3.2 Film swelling and water uptake

The degree of swelling of fibroin films was measured in terms of the equilibrium-swelling ratio of the films. Considering the possible applications of these biomaterials in artificial skin and wound dressings, the degree of swelling is one of the important factors in determining the usefulness of the biomaterials [41, 42]. The swelling experiments were conducted in phosphate buffered saline (pH 7.4). The fibroin films were treated with methanol prior to the studies. The weight of the completely dried sample and that of sample swollen in phosphate buffered saline at 37°C was measured at different time intervals after the removal of excess water. The swelling index of silk fibroin film fabricated from gland and cocoon was studied over a span of 24 h at an interval of 2 h (Fig. 3). The films were found to swell at an increasing rate for 8 h. After 8 h of incubation in phosphate buffered saline, the films did not show much change in water uptake. It may be concluded that the films show maximum uptake within initial 8 h. The fibroin films

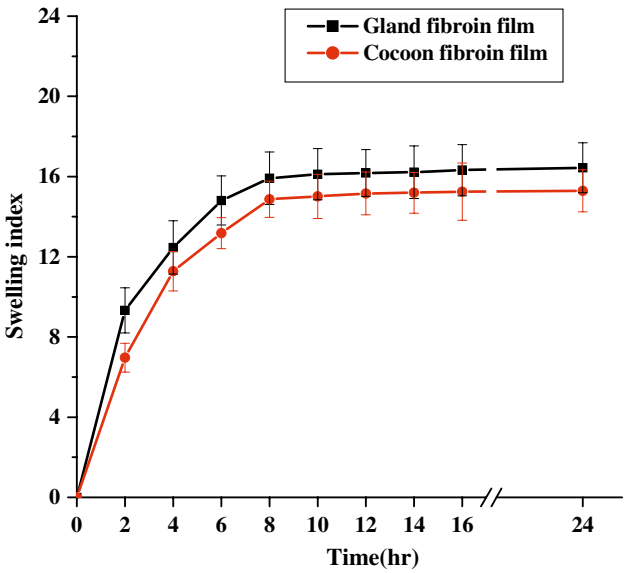

Fig. 3 Comparative swelling index (water uptake) of *Bombyx mori* gland and cocoon fibroin protein films

from the gland were found to possess slightly higher swelling index compared to that of cocoons. The swelling property of the films could be improved on blending with some polymers having higher water uptake like chitosan, PVA and Gelatin.

3.3 Fourier transform infrared spectroscopy (FTIR) analysis

One of the most important uses for regenerated silk fibroin solution is the manufacture of regenerated membranes or films. It is generally accepted that regenerated silk fibroin membranes cast from dilute silk fibroin solution obtained from cocoons and gland at room temperature show mostly random coil conformation. FTIR spectroscopy was performed and IR spectra of the regenerated fibroin films are shown in Fig. 4. Untreated gland showed strong absorption bands at 1650 (amide I), 1540 (amide II), and 1240 cm^{-1} (amide III), attributed to the random coil conformation. On the contrary, gland treated with methanol showed similar absorption bands at 1640 (amide I), 1540 (amide II), and 1240 cm^{-1} (amide III), assigned to the random coil conformation along with peaks at 1450 cm^{-1} (methanol group) which was absent in the untreated films and 1070 cm^{-1} (protein backbone stretching) compared to that of the 1170 cm^{-1} (C–O stretching vibrations) in the untreated films. The samples of *B. mori* cocoon fibroin films untreated showed strong absorption bands at 1655 (amide I), 1540 (amide II), and 1235 cm^{-1} (amide III), attributed to the random coil conformation [43, 44].

3.4 X-ray diffraction (XRD)

XRD is generally used to study the crystalline structure of the material [43]. There have been three types of crystalline structure proposed for silk. The glandular state prior to crystallization is called silk I. Silk II is the spun silk state which consists of the β-sheet secondary structure and silk III (an air/water assembled interfacial silk) which is a helical structure [45–47]. The main diffraction peaks of Silk I present at around $2\theta = 12.2$ and 28.2°, while Silk II present at about $2\theta = 18.9$ and 20.7° [48]. Pure silk fibroin film has a characteristic peak at $2\theta \approx 12.2°$, [17] which indicates Silk I structure. Methanol treated SF films, shows typical X-ray diffractograms of the β-sheet crystalline structure, since methanol is a crystallization inducing solvent [49]. Three distinct peaks were found in the X-ray diffractograms in the regions between 10 and 60°. Sharp peaks at $2\theta = 22.44°$ (Silk I conformation), 14.37 and 28.39 (both peaks denoting the silk II conformation) appeared in the XRD pattern of the films made from *B. mori* gland protein as shown in Fig. 5. The methanol treated films showed structural similarity with untreated films with peaks at $2\theta = 22.37°$ (Silk I conformation), 14.16° and 28.44° (both peaks denoting the silk II conformation). It can be concluded that amorphous silk fibroin is crystallized to β-sheet during processing of silk fibroin in the gland of *B. mori* 5th instar larvae.

3.5 Raman spectroscopy

The amide I and amide III bands of electrospun silk fibroin mats appeared at 1660, 1276, 1242 cm^{-1}, which suggests that electrospun fibroin mats are in random-coiled or silk I conformation. In addition, Raman spectra of electrospun silk

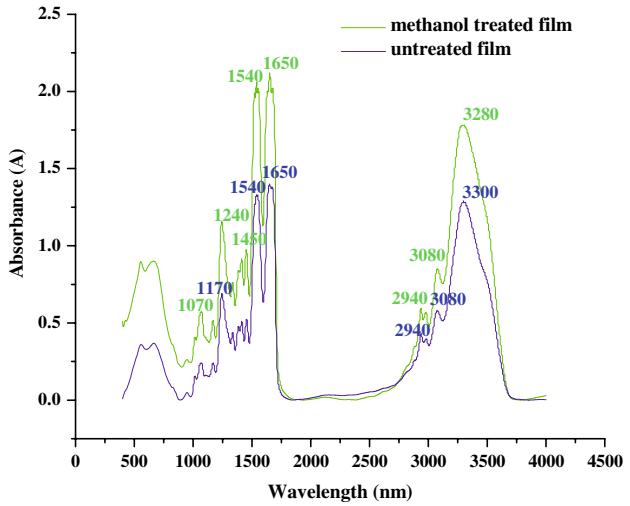

Fig. 4 The FTIR spectra of methanol treated and untreated films fabricated from *Bombyx mori* gland fibroin protein

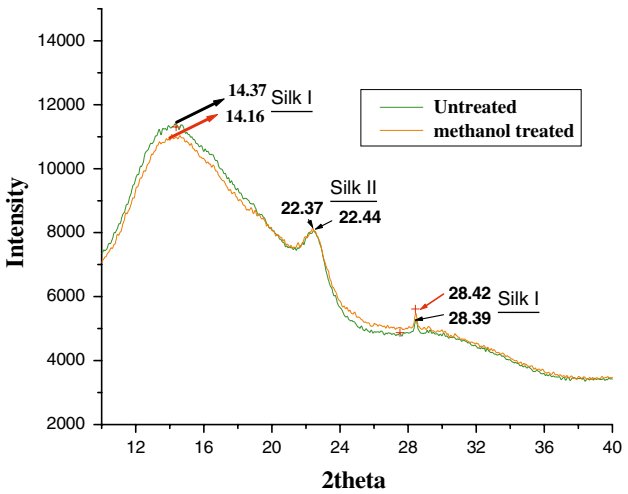

Fig. 5 X-ray diffraction analysis of methanol treated and untreated films fabricated from *Bombyx mori* gland fibroin protein

fibroin mats in C–C stretch range also had the peaks at 1107, 950 and 930, which is attributed to the silk I conformation [50]. The Raman spectra of *A. pernyi* fibroin appeared at 1667, 1224, 1242 cm^{-1} for amide I and amide III respectively [51]. According to our experiment results, as showed in Table 1 the Raman spectrum of *B. mori* silk gland fibroin methanol treated films exhibits strong bands near 1159 (CH ring in plane def., ring in plane def., δCH, NH3 oscillation.), 1525 (δ_{as}NH3, ν_{as}COO) and 1010 cm^{-1} (Ring in plane def., NH3 oscillation. δCH) respectively and weak bands at 1293 and 1617 cm^{-1} [52]. In Raman spectra of regenerated silk fibroin solution obtained by dissolving *B. mori* silk gland protein by lithium bromide several strong bands at 1157, 1523, 1007 cm^{-1} appear and weak bands at 1189 and 1342 cm^{-1} The results clearly indicated that the silk gland films on treatment with methanol undergoes Raman shift towards higher wave number. The peak intensity of the respective bands showed that the methanol treated films possessed higher intensity value compared to that of the untreated films possibly due to the higher degree of crystallinity found in the methanol treated films [53].

3.6 Atomic force microscopy (AFM)

The AFM provides a wealth of direct information about morphology with nanometer spatial resolution based on a novel principle that differs significantly from conventional microscopic and spectroscopic techniques. AFM images provided additional information related to the phase state and topography of silk gland fibroin films [4, 5]. AFM observation of the thin films of fibroin was performed to obtain further information on the microstructure of fibroin. It can be seen from the Fig. 6 that the fibroin molecules aggregated to form characteristic morphology (islands with branches). The morphological differences reflecting the secondary structures of the thick films are detected from the AFM plots. Before the treatment, the cast film with a secondary structure of the random coil type has a smooth surface. The root mean square (RMS) roughness in this case was 0.11 nm. After the methanol treatment, there has been induction of secondary structures, the film surface becomes somewhat rougher, and the RMS roughness in this case was 0.21 nm. Thus the driving force that induces the modification would be the adsorption of methanol followed by evaporation. Thus the surface topography of the fibroin film was affected by the treatments, leading to a conversion of the secondary structure.

3.7 Rheological properties of silk fibroin protein solutions

A few reports are available on the studies of the rheology of the regenerated silk fibroin solutions and for the first time we report the rheology of the regenerated silk fibroin solutions from the silk gland fibroin protein. Viscosity is a measure of the resistance of fluid to flow. Rheological behavior of polymer solutions is examined in order to determine the interaction between the polymer species and the solvent molecules. Shear viscosity of the silk fibroin solutions isolated from two different sources, namely *B. mori* cocoon and *B. mori* gland fibroin protein is plotted against the revolutions per minute at a constant torque percent (1%) and the relationship is shown in the Fig. 7. Both of the regenerated silk fibroin solutions showed evidently non Newtonian and shear thinning behavior [54]. The decrease in the shear viscosity of the fibroin aqueous solutions attributed towards entangled chains of polymer network within the solution. The results indicate that the shear viscosity profiles of the SF solutions of both sources are quite similar to each other indicating also higher degree of molecular entanglement within the regenerated solutions The *B. mori* fibroin molecule is a highly repetitive block copolymer in which highly ten hydrophobic blocks are separated by nine less hydrophobic blocks [39, 40]**.** The instability of the rheology at low shear rates results from an unstable balance between the

Table 1 Raman spectra band assignment for methanol treated and untreated *Bombyx mori* gland fibroin protein films

	Sample	Experimental value	Assignment
1	Methanol treated gland fibroin film	1159	CH ring in plane def., ring in plane def., δCH, NH3 oscillation
2		1525	δ_{as}NH3, ν_{as}COO, amide region
3		1010	Ring in plane def., NH3 oscillation., δCH
4		1293	τCH2, NH3 osc, δC6H15, νC7C8
5		1617	δ_{as}NH3, ν_{as}COO-aromatic ring stretching in phenyl alanine and tyrosine
6	Untreated gland fibroin film	1523	δ_{as}NH3, ν_{as}COO
7		1007	Ring in plane def., NH3 osc, δCH
8		1157	CH ring in plane def., ring in plane def., δCH, NH3 oscillation
9		1189	Aromatic C–H in plane blending
10		1342	CH3 symmetric bending, Hα bending

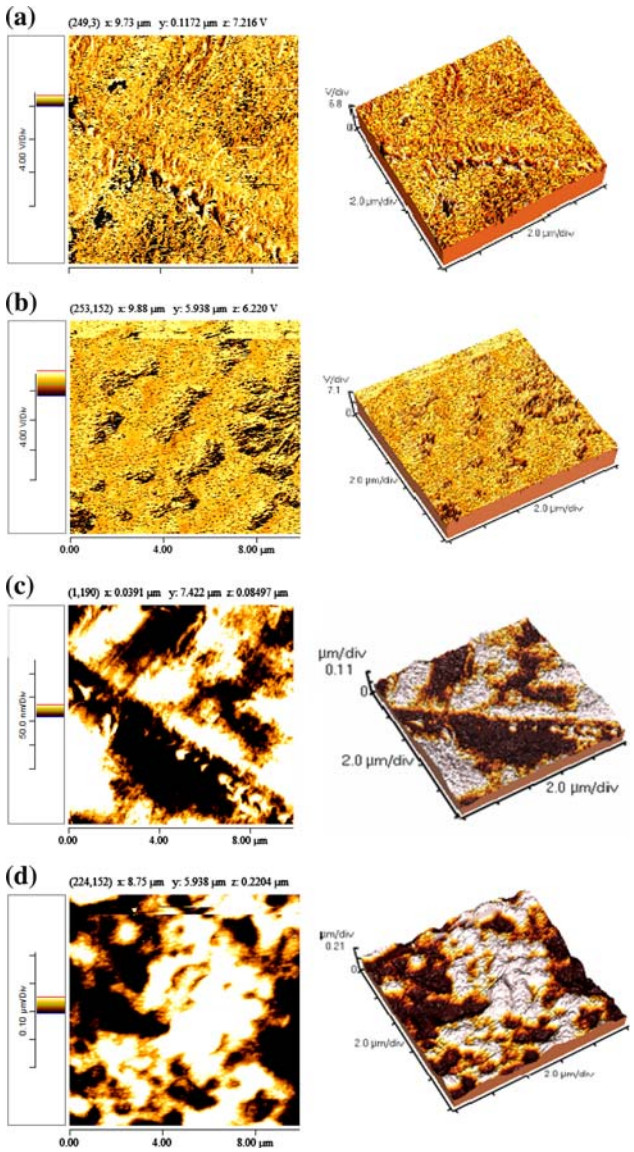

Fig. 6 AFM surface phase images of pure silk gland fibroin film (**a**) untreated; (**b**) methanol treated and surface topography images of pure silk gland fibroin film (**c**) untreated; (**d**) methanol treated. Scan range: 10 × 10 µm

shear tending to unwind the molecules and the effects of the solvent tending to return them to a compact coiled conformation. This unstable region in the rheology could account for the shear thinning behavior of the solutions [55]. The shear viscosity of the silk fibroin isolated from the gland showed similar rheological properties to that of the silk fibroin isolated from the *B. mori* cocoons.

3.8 Contact angle

Contact angle hysteresis is significantly influenced by the surface wetting behavior of a material. Static contact angle measurements do not provide information on contact angle

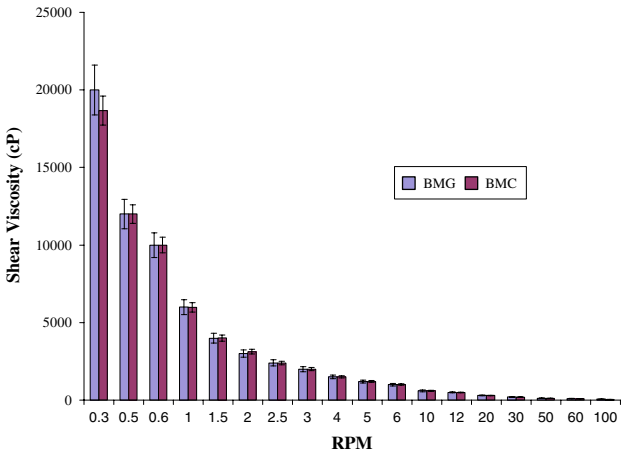

Fig. 7 Shear viscosity vs. speed (RPM) rate relationship of silk fibroin protein solutions of *Bombyx mori* silk gland and cocoon

hysteresis. Contact angle hysteresis is revealed by dynamic contact angle measurement. Contact angles of the native silk films of the gland and cocoon source were comparatively less hydrophobic. However, after methanol treatment, the contact angles of the films of the gland and cocoon source of silk proteins converged to around 65.22 ± 12.65° and 67.68 ± 14.58 (Table 2). These results were consistent with the surface structure properties of the films from both the sources. Water contact angles, particularly receding values in all cases were found to be very less as compared to that of the advancing contact angle. The solvents used in the experiments were distilled water. The change in the contact angle hysteresis attributes towards the surface roughness of the films [10, 56].

3.9 Mechanical properties

Force and elongation values were recorded and the values of tensile strength, percentage elongation-at-break and Young's modulus were calculated from the resulting

Table 2 Contact angle measurements of both methanol treated and untreated *Bombyx mori* fibroin protein films of glands and cocoons in distilled water

Sample name	Advancing contact angle	Receding contact angle	Average contact angle[a]
Gland fibroin film treated	74.17	56.28	65.22 ± 12.65
Cocoon fibroin film treated	78.18	57.18	67.68 ± 14.58
Gland fibroin film untreated	88.31	56.56	72.44 ± 22.45
Cocoon fibroin untreated	89.28	54.32	71.8 ± 23.44

[a] Average ± standard deviation ($n = 4$)

Table 3 Mechanical properties of *Bombyx mori* silk fibroin protein films (1% w/v)

Sample code	Sample thickness (μm)	Average tensile strength ± Stdev (MPa)	Modulus of elasticity ± Stdev (MPa)	% Elongation at break[a]
Gland fibroin film untreated	40	9.98 ± 2.33	177 ± 34.12	9.98
Gland fibroin film treated	40	14.29 ± 3.41	372 ± 44.12	11.52
Cocoon fibroin film untreated	40	8.09 ± 2.45	275 ± 30.12	10.77
Cocoon fibroin film treated	40	15. 09 ± 2.45	415 ± 40.12	13.77

[a] Mean value

stress–strain curve (also called force–deformation curve). Tensile strength was calculated by dividing the maximum load on the film before failure by the initial cross-sectional area (thickness × width). Percentage elongation-at-break was calculated by measuring the maximum extension of the film between the initial and final grip separation (35 mm). Young's modulus was calculated from the slope of the initial linear region of the force–deformation curve (at very small strain) [57]. The mechanical properties of silk fibroin films are shown in Table 3. Generally, the elastic value was closely correlated with the rigidity and crystallinity of silk fibroin. The fibroin films upon treatment with methanol were found to possess higher mechanical properties as compared to that of the untreated films. Both the fibroin films were found to possess more or less similar type of mechanical properties with that of from showed little higher values in all respect.

3.10 Thermogravimetric analysis (TGA)

Silk fibroin films cast from water solution contain bound water even after samples are dried in a vacuum oven. To remove the bound water, heat treatment at elevated temperatures is required. Bound water is lost from the film during heating, and the loss of mass is quantified using TGA. Bound water in the silk film acts as a plasticizer, and a lower glass transition temperature of the silk–water system. TGA results allow the water loss to be monitored quantitatively. Thermogravimetric curves of the regenerated SF films are shown in Fig. 8. The initial weight loss of SF films at ≈149.0°C is due to loss of moisture. The second weight loss took place in the temperature ranged from 218 to 330°C. This is associated with the breakdown of side chain groups of amino acid residues as well as the

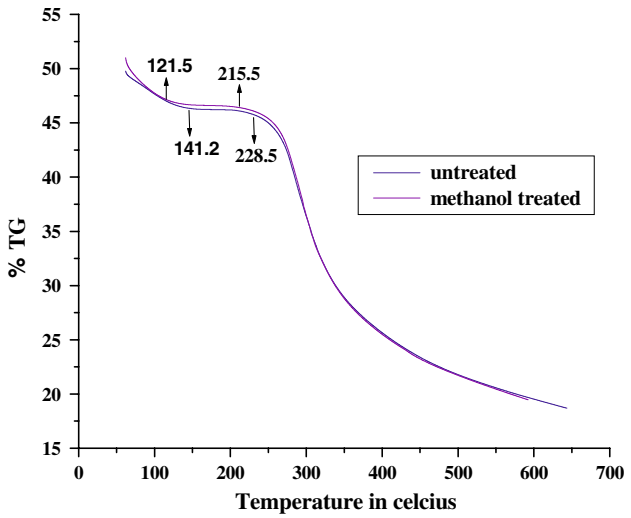

Fig. 8 Thermogravimetric analysis of methanol treated and untreated films of *Bombyx mori* gland fibroin protein

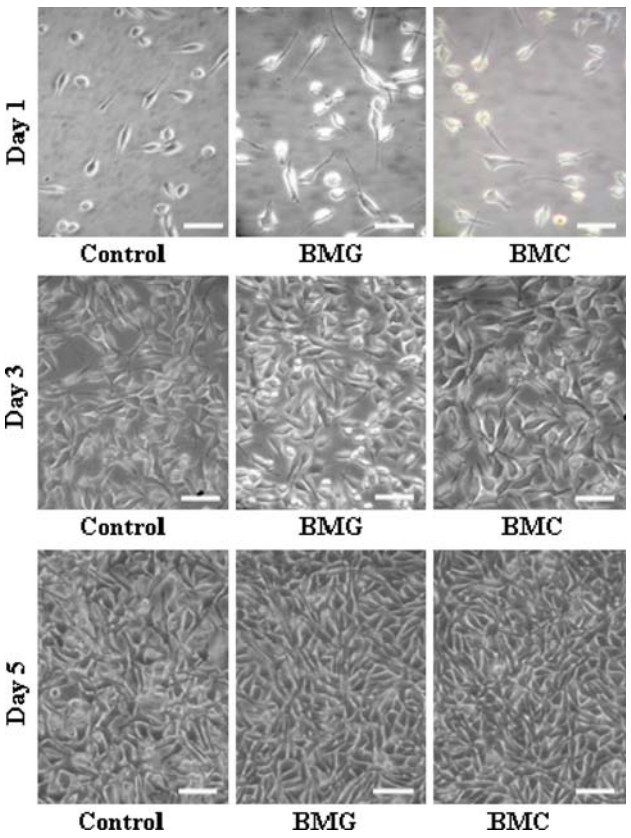

Fig. 9 L929 fibroblast Cell morphology on control, pure silk gland protein fibroin film (treated), pure silk cocoon fibroin protein film after day 1, day 3 and day 5 of cell culture, Scale bar = 100 μm

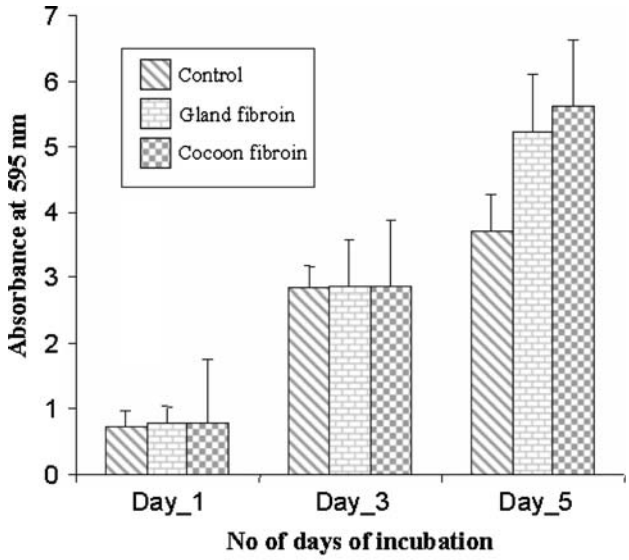

Fig. 10 MTT assay of L929 fibroblast cells on control, pure silk gland protein fibroin film (methanol treated), and pure silk cocoon protein fibroin film (methanol treated) after day 1, day 3 and day 5 of cell culture ($n = 3$). Each point on the curve represents an average of three experiments ±SD. ($P < 0.05$)

cleavage of peptide bonds. The amorphous sample showed faster degradation curve, indicating lower thermal stability than other crystalline sample having a β-sheet structure. The differential thermal analysis plots of the untreated and treated films showed two (at 287 and 306°C) and three peaks (at 286, 305 and 325°C) respectively.

3.11 Cell culture and MTT assay

The proliferation and cell viability of L929 mouse fibroblast cells on fibroin isolated from the 5th instar mature larval gland and cocoons of *B. mori* coated polystyrene tissue culture plates were cultured for 1, 3 and 5 days was compared by MTT assay. The morphology of the cells as seen in the Fig. 9 reveals that L929 mouse fibroblast cell adhered to the protein surfaces and also spread properly. The coated surfaces were found to be confluent within 5 days of incubation of 10,000 cells on day zero in 6-well tissue culture plates and thus signify that the cells proliferated very well on these surfaces. The MTT results as in Fig. 10 shows that the biocompatibility of the silk film obtained from both the sources is found to possess more or less similar non-toxic behavior.

4 Conclusion

The study outlines the properties of mulberry non-engineered silk fibroin protein obtained from silk gland of 5th instar larvae not allowing the silk worm to biospinning into cocoon as biomaterial matrices. The turbidity of silk fibroin aqueous solutions increased with increase in the protein concentration. Similar to the cocoon protein aqueous fibroin the silk gland fibroin aqueous solutions showed non Newtonian and shear thinning behavior. The spectroscopy studies of the silk gland fibroin films shows the presence of amide I, amide II and amide III peaks and the conformational transition from random coil to β-sheet on methanol treatment. The Raman spectroscopy results showed strong peaks in regions 1157, 1523, 1007 cm^{-1} which are absent in the silk cocoon fibroin films. X-ray diffraction studies of the films showed peaks at $2\theta = 22.37°$ (Silk I conformation), 14.16 and 28.44° (both peaks denoting the silk II conformation) on treatment with methanol and showed very less difference with the untreated films. The XRD diffraction profiles were different from the pattern obtained from films of silk fibroin from cocoons. For biomedical application both the films were comparable and possess the necessary properties and characteristics of a good biomaterial. Treatments of the films were necessary as the films undergo structural conformation from amorphous and random coil to beta sheet conformation. This adds to the stability of the films. Biomaterial used in clinical should have good properties in bulk as well as on the surface. The biomaterial surface first comes into contact with the living tissues when the biomaterial is planted in the body. The initial response of the body to the biomaterial depends on its surface properties. Surface properties like surface topography, contact angle and surface charge influence the biocompatibility. The biomaterial should possess good tensile and mechanical characteristics similar to that of the living tissue to be replaced. Both the biocompatibility and the mechanical properties of biomaterials are important in biomaterial applications. The silk gland fibroin protein two dimensional matrices may also be considered as potential biomaterial by virtue of its good mechanical strength, water stability and swelling index, thermal properties, surface roughness, biocompatibility as these characteristics are essential for tissue engineering applications.

Acknowledgements Financial support was obtained from Indo-Australia Biotechnology Fund and Department of Biotechnology, Government of India, New Delhi.

References

1. K. Grzelak, Comp. Biochem. Physiol. B: Biochem. Mol. Biol. **110**, 671 (1995)
2. T. Gamo, Biochem. Genet. **20**, 165 (1982)
3. J.J. Michaille, P. Couble, J.C. Prudhomme, A. Garel, Biochimie **68**, 1165 (1986)
4. S. Inoue, K. Tanaka, F. Arisakaffi, J. Biol. Chem. **275**, 40517 (2000)
5. S. Inoue, J. Magoshi, T. Tanaka, Y. Magoshi, M. Becker, J. Polym. Sci., Part B, Polym. Phys. **38**, 1436 (2000)

6. K. Hu, Q. Lv, F. Cui, Q. Feng, X. Kong, H. Wang, J. Bioact. Compat. Polym. **21**, 23 (2006)
7. T. Arai, G. Freddi, R. Innocenti, M. Tsukada, J. Appl. Polym. Sci. **91**, 2383 (2004)
8. G.H. Altman, F. Diaz, C. Jakuba, T. Calabro, R.L. Horan, J. Chen, Biomaterials **24**, 401 (2003)
9. C. Vepari, D.L. Kaplan, Prog. Polym. Sci. **32**, 991 (2007)
10. S. Hofmann, C.T. Wong Po Foo, F. Rossetti, M. Textor, G. Vunjak-Novakovic, D.L. Kaplan, H.P. Merkle, L. Meinel, J. Control Release **111**, 219 (2006)
11. M. Fini, A. Motta, P. Torricelli, G. Giavaresi, N. Nicoli Aldini, M. Tschon, R. Giardino, C. Migliaresi, Biomaterials **26**, 3527 (2005)
12. T. Hino, M. Tanimoto, S. Shimabayashi, J. Colloid Interface Sci. **266**, 68 (2003)
13. J. Zhu, H. Shao, X. Hu, Int. J. Biol. Macromol. **41**, 469 (2007)
14. A. Sugihara, K. Sugiura, H. Morita, T. Ninagawa, K. Tubouchi, R. Tobe, Proc. Soc. Exp. Biol. Med. **225**, 58 (2000)
15. Y. Wang, D.J. Blasioli, H.J. Kim, H.S. Kim, D.L. Kaplan, Biomaterials **27**, 4434 (2006)
16. S. Rammensee, D. Huemmerich, K.D. Hermanson, T. Scheibel, A.R. Bausch, Appl. Phys. A **82**, 261 (2006)
17. X.X. Feng, L.L. Zhang, J.Y. Chen, Y.H. Guo, H.P. Zhang, C.I. Jia, Int. J. Biol. Macromol. **40**, 105 (2007)
18. S. Putthanarat, S. Zarkoob, J. Magoshi, J.A. Chen, R.K. Eby, M. Stone, W.W. Adams, Polymer **43**, 3405 (2002)
19. N. Agarwal, D.A. Hoagland, R.J. Farris, J. Appl. Polym. Sci. **63**, 401 (1997)
20. Y.Y. Sun, Z.Z. Shao, M.H. Ma, P. Hu, Y.S. Liu, T.Y. Yu, J. Appl. Polym. Sci. **65**, 959 (1997)
21. M.Z. Li, Z.Y. Wu, C.S. Zhang, S.Z. Lu, H.J. Yan, D. Huang, H.L. Ye, J. Appl. Polym. Sci. **79**, 2192 (2001)
22. A.B. Mathur, A. Tonelli, T. Rathke, S. Hudson, Biopolymer **42**, 61 (1997)
23. S. Gobin, V.E. Froude, A.B. Mathur, J. Biomed. Mater. Res. A. **74**, 465 (2005)
24. K.E. Park, S.Y. Jung, S.J. Lee, B.M. Min, W.H. Park, Int. J. Biol. Macromol. **38**, 165 (2006)
25. X. Wang, H.J. Kim, P. Xu, A. Matsumoto, D.L. Kaplan, Langmuir **21**, 11335 (2005)
26. R. Nazarov, H.J. Jin, D.L. Kaplan, Biomacromolecules **5**, 718 (2004)
27. R. Valluzzi, S.P. Gido, W. Muller, D.L. Kaplan, Int. J. Biol. Macromol. **24**, 237 (1999)
28. X. Wang, H.J. Kim, P. Xu, A. Matsumoto, D.L. Kaplan, Langmuir **21**, 11335 (2005)
29. J.S. Hwang, J.S. Lee, T.W. Goo, E.Y. Yun, K.S. Lee, Y.S. Kim, B.R. Jin, S.M. Lee, K.Y. Kim, S.W. Kang, D.S. Suh, Biotech. Lett. **231**, 1321 (2001)
30. W. Wang, S. Zhu, L. Wang, F. Yu, W. Shen, J. Biosci. **30**, 605 (2005)
31. B.B. Mandal, S.C. Kundu, Biotechnol.Bioeng. in press
32. H. Shiozaki, Y. Tanaka, Angewandte Makromolekulare Chemie **64**, 1 (2003)
33. M.L. Gimenes, L. Liu, X. Feng, J. Memb. Sci. **29**, 71 (2007)
34. X. Wang, X. Hu, A. Daley, O. Rabotyagova, P. Cebe, D.L. Kaplan, J. Control Release **121**, 190 (2007)
35. O. Bayraktar, Ö. Malay, Y. Özgarip, A. batigün, Eur. J. Pharm. Biopharm. **60**, 373 (2005)
36. H.J. Jin, J. Park, V. Karageorgiou, U.J. Kim, R. Valluzzi, P. Cebe, D.L. Kaplan, Adv. Func. Mater. **15**, 1241 (2005)
37. ASTM, *Annual Book of ASTM Standards*. (Philadelphia, PA, USA, 1993), p. 59
38. O. Malay, O. Bayraktar, A. Batiguin, Int. J. Biol. Macromol. **40**, 387 (2007)
39. D.L. Kaplan, S. Fossey, C.M. Mello, Mat. Res. Soc. Bull. **17**, 41 (1992)
40. C.Z. Zhou, F. Confalonieri, N. Medina, Y. Zivanovic, C. Esnault, T. Yang, M. Jacquet, J. Janin, M. Duguet, R. Perasso, Z.G. Li, Nucleic Acids Res. **28**, 2413 (2000)
41. J.H. Yeo, K.G. Lee, Y.W. Lee, S.Y. Kim, Eur. Polym. J. **39**, 1195 (2003)
42. M.K. Yoo, H.Y. Kweon, K.G. Lee, H.C. Lee, C.S. Cho, Int. J. Biol. Macromol. **34**, 263 (2004)
43. I.C. Um, H.Y. Kweon, Y.H. Park, S. Hudson, Int. J. Biol. Macromol. **29**, 91 (2001)
44. H. Wang, Y. Zhang, H. Shao, X. Hu, Int. J. Biol. Macromol. **36**, 66 (2005)
45. D.L. Kaplan, S.M. Mello, S. Arcidiacono, S. Fossey, K.W.M. Senecal, *Protein Based Materials*. (Birkhauser, Boston, 1998), p. 103
46. H.J. Jin, D.L. Kaplan, Nature **424**, 1057 (2003)
47. A. Motta, L. Fambri, C. Migliaresi, Macromol. Chem. Phys. **203**, 1658 (2002)
48. N. Miniura, S. Aiba, M. Higuchi, Biochem. Biophys. Res. Comm. **208**, 511 (1995)
49. M. Tsukada, Y. Gotoh, M. Nagura, N. Minoura, N. Kasai, G. Freddi, J. Polym. Sci. B: Polym. Phys. **32**, 961 (1994)
50. J. Zhu, H. Shao, X. Hu, Int. J. Biol. Macromol. **41**, 469 (2007)
51. W. Tao, M. Li, C. Zhao, Int. J. Biol. Macromol. **40**, 472 (2007)
52. T. Iliescu, D. Maniu, V. Chis, F.D. Irimie, C.S. Paizs, M. Tosa, Chem. Phys. **310**, 189 (2005)
53. M.E. Rousseau, T. Lefèvre, L. Beaulieu, T. Asakura, M. Pézolet, Biomacromolecules **56**, 2247–2257 (2004)
54. J.W. Van Egmond, Curr. Opin. Colloid Interface Sci. **3**, 385 (1998)
55. X. Chen, D.P. Knight, Z. Shao, F. Vollrath, Polymer **42**, 9969 (2001)
56. K. Cai, K. Yao, Y. Cui, Z. Yang, X. Li, H. Xie, T. Qing, L. Gao, Biomaterials **23**, 1603 (2002)
57. A.M. Tellez-Garay, M.Sc. Thesis, Texas A&M University, College Station, TX (1999)